arXiv:1101.4432v1 [astro-ph.SR] 24 Jan 2011

Spectroscopic Studies of Extremely Metal-Poor Stars with the Subaru High Dispersion Spectrograph. V. The Zn-Enhanced Metal-Poor Star BS 16920–017[1]

Satoshi Honda[2,3], Wako Aoki[4,5], Timothy C. Beers[6], Masahide Takada-Hidai[7]

ABSTRACT

We report Zn abundances for 18 very metal-poor stars studied in our previous work, covering the metallicity range $-3.2 <$ [Fe/H] < -2.5. The [Zn/Fe] values of most stars show an increasing trend with decreasing [Fe/H] in this metallicity range, confirming the results found by previous studies. However, the extremely metal-poor star BS 16920–017 ([Fe/H]= -3.2) exhibits a significantly high [Zn/Fe] ratio ([Zn/Fe] = $+1.0$). Comparison of the chemical abundances of this object with HD 4306, which has similar atmospheric parameters to BS 16920–017, clearly demonstrates a deficiency of α elements and neutron-capture elements in this star, along with enhancements of Mn and Ni, as well as Zn. The association with a hypernova explosion that has been proposed to explain the high Zn abundance ratios found in extremely metal-poor stars is a possible explanation, although further studies are required to fully interpret the abundance pattern of this object.

Subject headings: nuclear reactions, nucleosynthesis, abundances — stars: abundances — stars: Population II — supernovae: general — stars: individual (BS 16920–017)

1. Introduction

The chemical compositions of very metal-poor stars have been intensively investigated to provide observational constraints on the yields of early generations of massive stars and the result-

[2]Gunma Astronomical Observatory, Takayama-mura, Agatsuma, Gunma 377-0702, Japan

[3]Current address: Kwasan Observatory, Kyoto University, Ohmine-cho Kita Kazan, Yamashina-ku, Kyoto, 607-8471, Japan; honda@kwasan.kyoto-u.ac.jp.

[4]National Astronomical Observatory, Osawa, Mitaka, Tokyo, 181-8588 Japan; email: aoki.wako@nao.ac.jp

[5]Department of Astronomical Science, School of Physical Sciences, The Graduate University of Advanced Studies, Mitaka, Tokyo 181-8588, Japan;

[6]Department of Physics & Astronomy and JINA: Joint Institute for Nuclear Astrophysics, Michigan State University, East Lansing, MI 48824-1116; email: beers@pa.msu.edu

[7]Liberal Arts Education Center, Tokai University, Hiratsuka, Kanagawa, 259-1292, Japan; email: hidai@apus.rh.u-tokai.ac.jp

[1]Based on data collected at the Subaru Telescope, which is operated by the National Astronomical Observatory of Japan.

ing elemental enrichment in the Galaxy. In particular, extremely metal-poor stars (EMP; [Fe/H] < -3)[2] have been argued to reflect the result of individual nucleosynthesis processes associated with the supernovae explosions of early generation stars (e.g., Beers & Christlieb 2005).

Zinc, along with Ge, is often considered the heaviest of the Fe-peak elements, and its production by core-collapse supernovae is expected to be dependent on details of the explosions. Observational studies in the past decades have revealed a clear increasing trend of [Zn/Fe] ratios with decreasing metallicity in the range of [Fe/H]$\lesssim -2.5$ (e.g., Cayrel et al. 2004). Such a trend could not be explained by previously studied core-collapse supernova models. Thus, large contributions of energetic supernovae, called hypernovae, have been suggested as a possible source of the higher [Zn/Fe] ratios in the early stages of chemical enrichment of the Galaxy (Umeda & Nomoto 2002). Chemical evolution models including hypernovae yields reproduce, at least qualitatively, the observed trend of [Zn/Fe] at very low metallicity (e.g., Kobayashi et al. 2006; Tominaga et al. 2007). Other scenarios to explain Zn excesses at extremely low metallicity have been also discussed. For example, Zn might be also synthesized by neutron-capture processes during helium burning in the shells of low- to intermediate-mass AGB stars (main s-process) and in the cores of massive stars (weak s-process) , as has been investigated by Baraffe et al. (1992), Matteucci et al. (1993), and Raiteri et al. (1993). However, it remains unclear how effective these contributions might be at extremely low metallicity.

Another interesting observational result on Zn abundances at very low metallicity is the rather small scatter of [Zn/Fe] ratios. The abundance ratios among Fe-peak elements, e.g., [Cr/Fe] and [Ni/Fe], in metal-poor red giants exhibit clear trends with little scatter (Cayrel et al. 2004; Lai et al. 2008), although some of them simply trace the solar abundance ratio. The small observed scatter in the [Zn/Fe] ratios is perhaps surprising, given the expected sensitivity of the yields of Fe-peak nuclei to the parameters used to model explosive nucleosynthesis. It should also be noted that the heavy neutron-capture elements (e.g., Sr, Ba, Eu; $Z \geq 38$), which are also thought to be produced during the explosion of core-collapse supernovae, exhibit a very large scatter in their abundance ratios (e.g. McWilliam et al. 1995; Honda et al. 2004b). No clear excess of Zn is found for objects that show large enhancements of heavy neutron-capture elements (Cayrel et al. 2004; François et al. 2007), nor of light ones (Honda et al. 2006, 2007).

Although the [Zn/Fe] ratios in the Galactic halo exhibit a clear trend with little scatter, a few stars are known that have exceptionally low or high Zn abundances. Ivans et al. (2003) investigated three halo stars with unusually low α-element abundances, and reported one with a low [Zn/Fe] abundance ratio, while the remaining two have quite high values. Moreover, the Zn abundances of intermediate and higher metallicity stars in dwarf satellites around the Galaxy appear systematically lower than those of field stars (e.g., Cohen & Huang 2010). These observations indicate that further investigations to understand the origins of Zn, and its implications for the

[2]We use the usual notation [A/B]$\equiv \log_{10}(N_A/N_B)_* - \log_{10}(N_A/N_B)_\odot$ and $\log\epsilon(A) \equiv \log_{10}(N_A/N_H) + 12.0$, for elements A and B. Also, the term "metallicity" will be assumed here to be equivalent to the stellar [Fe/H] value.

chemical evolution of the Galaxy (as well as in dwarf galaxies), are strongly desired.

In this paper we report our measurements of Zn abundances for the sample of very metal-poor stars studied by Honda et al. (2004b). Among them, one star (BS 16920–017) turned out to have an exceptionally high [Zn/Fe] ratio. The detailed chemical abundance pattern of this object, determined by an abundance analysis relative to an object having similar atmospheric parameters (HD 4306), is also reported. Our observations and measurements are summarized in Section 2. In Section 3, details of the abundance analyses and the results are reported. The significance of the Zn excess in BS 16920–017 and its implications are discussed in Section 4.

2. Observations and Measurements

Zinc abundances are determined from the high-resolution spectra reported in Honda et al. (2004a,b) (hereafter, Paper I and II, respectively), which were obtained with the High Dispersion Spectrograph (HDS; Noguchi et al. 2002) of the Subaru Telescope (Table 1). The spectra cover the wavelength range 3500–5100 Å, including the two Zn I lines at 4722 Å and 4810 Å, with a resolving power of $R = 50,000$. Details of the observations have been reported in Paper I.

The signal-to-noise ratio of the previous spectrum of BS 16920–017 was not as high as the average of other stars in the sample of Honda et al. (2004a). In addition, the Zn I 4810 Å line of this object was affected by a bad column on the CCD. In order to improve the data quality around the Zn lines, another spectrum of BS 16920–017 was obtained with the same instrument, covering 4030 Å to 6800 Å, with a resolving power of $R = 60,000$, in May 2004. The observation details are given in Table 1.

Standard data reduction procedures (bias subtraction, flat-fielding, background subtraction, extraction, and wavelength calibration) are carried out with the IRAF echelle package[3], as described in Paper I and Aoki et al. (2005, Paper III).

Equivalent widths of the two Zn I lines were measured by the fitting of Gaussian profiles; results of this exercise are listed in Table 2. In order to investigate the relative abundances for BS 16920–017 and HD 4306, equivalent widths of other elements were measured for a common line set for these two stars. The line data are adopted from Paper III and Aoki et al. (2007, Paper IV). The gf values of Zn I are obtained from Biemont & Godefroid (1980). In the lines of this list, the effect of hyperfine splitting in some Mn and Ba lines is significant. While the effect of hyperfine splitting was included in the Ba analysis in Paper II, it was not for the Mn lines. Here we take this effect into account for the Mn analysis, using the line data of McWilliam et al. (1995). The full line list and measured equivalent widths are listed in Table 3.

[3]IRAF is distributed by the National Optical Astronomy Observatories, which is operated by the Association of Universities for Research in Astronomy, Inc. under cooperative agreement with the National Science Foundation.

Since the spectral resolution and on-chip binning mode used to obtain the two spectra of BS 16920–017 are different, they were not merged in the present analysis. For the abundance analysis from lines in the overlapping wavelength range, priority is given to previous measurements (Paper I). For HD 4306, we adopted the equivalent widths measured by McWilliam et al. (1995) for the red range, which was not covered by our previous observations. Although the quality of the data of McWilliam et al. (1995) is not as high as that of our Subaru spectra in general, their red spectrum of the bright giant HD 4306 has sufficient quality for our purposes. Our measurements of equivalent widths for HD 4306 exhibit no systematic difference from those of McWilliam et al. (1995) for the wavelength range in common (see Fig. 6 of Paper I).

Radial velocities are measured using clean Fe I lines. The results are given in Table 1, along with the observing date for each spectrum. No significant change of heliocentric radial velocity is found for BS 16920–017 between the two observations in April 2001 and May 2004. Prior to our observations, Allende Prieto et al. (2000) obtained a radial velocity of this star (–210 ± 10 km s^{-1}) based on medium-resolution ($R = 2000$) spectra. This value agrees with our result within their reported measurement error. Hence, there exists no evidence of binarity for BS 16920–017 based on the data obtained thus far.

3. Abundance Analyses and Results

As was done in Paper II, chemical abundance analyses are performed using the analysis tool SPTOOL developed by Y. Takeda (Takeda 2005, private communication), based on Kurucz's ATLAS9/WIDTH9 program (Kurucz 1993). SPTOOL calculates synthetic spectra and equivalent widths of lines on the basis of the given atmospheric parameters, line data, and chemical composition, under the assumption of LTE.

We adopted the model atmosphere parameters (Table 4; effective temperature, surface gravity, microturbulent velocity, and metallicity) derived in Paper II, and listed in Table 2 of that paper. In the previous study, the effective temperature ($T_{\rm eff}$) was derived from photometric data (primarily $V - K$), adopting the temperature scale of Alonso et al. (1996). The microturbulent velocity ($v_{\rm micro}$) and the surface gravity ($\log g$) are determined from the usual constraint that the abundances derived from individual Fe I and Fe II lines are consistent with one another. The iron abundance ([Fe/H]) is adopted as the metallicity; the [Fe/H] derived from Fe I and Fe II lines are equivalent within the reported errors.

Cayrel et al. (2004) and Roederer et al. (2010) pointed out that the abundance of Mn derived from the resonance triplet at 4030 Å is systematically lower ($\sim$ 0.4 dex) than the abundance from the other Mn lines. Our results for the abundance analysis in BS 16920–017 and HD 4306 show the same trend. If we also adopt the correction of 0.4 dex for the abundance from the triplet lines, the result is in good agreement with the abundance derived from the other Mn lines. In that case, the derived abundance of Mn in HD 4306 is in agreement with previous studies (Paper II, McWilliam

et al. 1995). However, the cause of this difference remains as a matter to be discussed further. In this paper, we adopted the mean value of 6 lines with individually large errors.

3.1. Zinc Abundances for 18 Very Metal-Poor Stars

We use the two Zn I lines at 4722 Å and 4810 Å for the determination of Zn abundances; the region of the Zn I 4722 Å line for several spectra is shown in Figure 1. Contamination from other spectral lines is not evident at the wavelengths of these two lines in very metal-poor stars. The measured equivalent widths and the abundances from individual lines are listed in Table 2. In general, we adopt the straight mean of the results from the two lines as the final result for the Zn abundance. An exception is CS 30306–132, for which only the 4722 Å line is covered by our spectrum. The three stars BS 16082–129, CS 22892–052, and CS 22952–015 exhibit large discrepancies ($\sim$ 0.3 dex) between the abundances derived from the two lines. Moreover, the equivalent widths of the 4722 Å line are larger than those of the 4810 Å in these three stars, even though the $\log gf$ value of the 4810 Å line is greater than that of the other line. Sneden et al. (2003) measured the 4810 Å line of CS 22892–052 to be 8 mÅ, which is in agreement with our value (9.2 mÅ). The equivalent width of the 4810 Å line of CS 22952–015 measured by Cayrel et al. (2004) (5.3 mÅ) is smaller than our measured value (8.5 mÅ), but this discrepancy can be fully accounted for by the reported measurement error (3.2 mÅ for weak lines, see Paper I). This gives us confidence in our measurement of the 4810 Å line rather than the 4722 Å line. Therefore, for these three stars we adopt the Zn abundance from the 4810 Å line as the final result. Excluding the above three objects, the offset of the mean abundances from the two spectral lines is only 0.014 $\pm$0.016 dex, which is much smaller than the scatter of the abundance differences from the two lines (0.062 dex).

Two sources of errors are included in our estimates of the accuracy for our derived abundances. One is random errors, which might be caused by the adopted line data and equivalent width measurements. The size of the random errors are estimated from the mean of the standard deviations (1 σ) of the abundances derived from individual lines for elements that had three or more lines available. Another source is errors arising from uncertainties in the adopted atmospheric parameters. The effect on the [Zn/Fe] values is estimated by changing the atmospheric parameters for BS 16920–017 as follows; $\Delta\ T_{\rm eff} = 100$ K (Δ[Zn/Fe] = 0.04 dex), $\Delta\ v_{\rm micro} = +0.3$ dex (0.08 dex), $\Delta \log g = +0.5$ dex (0.02 dex), and Δ [Fe/H] = +0.3 dex (0.05 dex).

The derived Zn abundances are plotted in Figure 2, along with the results obtained by previous studies. Sneden et al. (1991) investigated the Zn abundances of stars with [Fe/H] $\simeq$ –3, and showed that most objects exhibit solar ratios of [Zn/Fe]. However, Primas et al. (2000) investigated Zn abundances for a larger sample, and found that a few very metal-poor stars exhibit over-abundances of [Zn/Fe]. This trend becomes clearer from the observations of Cayrel et al. (2004) and Nissen et al. (2007). Our study confirms the increasing trend of [Zn/Fe] with decreasing metallicity for [Fe/H] < -2.5. We note that non-LTE corrections for the Zn lines we have employed are

quantitatively not significant for the stars in our sample (Takeda et al. 2005). Energetic core-collapse supernovae (hypernovae) are suggested to be a possible origin of these Zn excesses (see Section 4).

By contrast to the clear trend of [Zn/Fe] with declining [Fe/H] and the small associated scatter, BS 16920–017 exhibits a very large abundance of Zn ([Zn/Fe] = +1 at [Fe/H] = –3), higher than reported among very metal-poor stars by previous studies (Cayrel et al. 2004; Nissen et al. 2007). In the sample of Cayrel et al. (2004), [Zn/Fe] reaches to $\sim +0.7$ at [Fe/H]$=-4$. In order to investigate the significance of the Zn excess in BS 16920–017, the average and scatter of [Zn/Fe] are calculated for metallicity bins of Δ[Fe/H] = 0.2 (Figure 2). The average [Zn/Fe] at [Fe/H] = –3.0 is +0.33 with the standard deviation of 0.13 dex in our sample, while they are +0.23 and 0.12 dex, respectively, for the entire sample shown in Figure 2. These averages are also in agreement with the result of Saito et al. (2009) for metallicity bins of Δ [Fe/H] = 0.5 dex.

At higher metallicity ([Fe/H] ~ -2), two halo stars with exceptionally large Zn abundances were reported by Ivans et al. (2003) (G 4–36 and CS 22966–043; [Zn/Fe] $\simeq$+1). Both of these metal-poor stars exhibit low abundances of their α elements and neutron-capture elements, along with high abundances of Fe-peak elements. We discuss comparisons of BS 16920–017 with those two stars in Section 4.

3.2. Relative Abundances of BS 16920–017 with respect to HD 4306

In an attempt to elucidate the reason for the very high [Zn/Fe] abundance ratio in BS 16920–017, we investigate the detailed abundance patterns of other elements for this object (Table 5). To avoid the systematic errors in the abundance analyses, such as possible non-LTE effects and uncertainties in the adopted temperature scale, we select HD 4306 as a reference star, and performed abundance analyses using a common line list. HD 4306 is a bright very metal-poor star having similar stellar parameters to BS 16920–017, and it exhibits a typical elemental abundance pattern found in very metal-poor stars (Paper II).

While the difference in metallicity ([Fe/H]) between the two stars is about 0.3 dex, larger differences are seen between other elements. The differences are also evident from direct inspection of the spectra (see Figures 3-5). The abundance patterns of the two stars are shown in Figure 6; the lower panel depicts the abundance differences, on the logarithmic scale, between the two stars.

As an overall trend, BS 16920–017 exhibits higher abundances of its iron-peak elements, compared with its α elements and neutron-capture elements, relative to HD 4306. Mn, Ni, and Zn have remarkably high values compared to Cr, Fe, and Co. On the other hand, the abundances of the α elements (Mg, Si, Ca), as well as Na and Sc, in BS 16920–017 are deficient compared with those of HD 4306. The neutron-capture elements Sr and Ba also exhibit significant under-abundances. The Ba abundance of BS 16920–017 is among the lowest values found by previous studies of very metal-poor stars (e.g., Honda et al. 2004b; François et al. 2007).

Given the low [α/Fe] ratio found in BS 16920–017 with respect to other EMP stars (see below), it may be interesting to adopt the α elements as the metallicity reference in such comparisons. While most objects shown in Figure 2 have over-abundances of their α elements ([α/Fe] $\sim +0.3$; Paper II), that of BS 16920–017 is close to the solar ratio ([α/Fe]$= +0.03$), resulting in [α/H]~ -3. Excluding BS 16920–017, the [Zn/Fe] at [α/H]$= -3.0$ ([Fe/H]~ -3.3) is slightly higher than that at [Fe/H]$= -3.0$ on average. However, the large enhancement of Zn in BS 16920–017 is still evident even at this value of [α/H]. We note for completeness that the Zn excess of BS 16920–017 is more significant in the comparisons of [Zn/α] at [α/H]~ -3.

4. Discussion and Concluding Remarks

We have derived Zn abundances for 18 very metal-poor stars ([Fe/H] < -2.5). We confirm the increasing trend of [Zn/Fe] with decreasing metallicity, with little dispersion, as found by previous studies. Although Zn is usually classified as an iron-peak element, its origin is still not well understood. The nucleosynthesis of Zn is thought to be the result of complete Si burning and neutron-capture processing (e.g., Heger & Woosley 2002; Umeda & Nomoto 2002). Recently, the trend of increasing [Zn/Fe] with decreasing metallicity has been shown to be consistent with chemical evolution models including the contributions of hypernovae (e.g., Kobayashi et al. 2006; Tominaga et al. 2007). On the other hand, Heger & Woosley (2010) concluded that the elemental abundance ratios of EMP stars are explained by their supernovae models without a hypernova component, assuming the production and ejection of Zn in neutrino-driven winds from a proto-neutron star (e.g., Pruet et al. 2005) or the accretion disk of a black hole (e.g., Fröhlich et al. 2006). However, their models predict lower Co and Zn abundances than observed, and they will not be enhanced by the ejecta from the innermost layers (Izutani & Umeda 2010).

We found that one star in our sample, BS 16920–017, exhibits [Zn/Fe] $= +1.04$, substantially larger than the average [Zn/Fe] for other stars with metallicity near [Fe/H] $= -3.0$. The overall elemental abundance pattern of BS 16920–017, that is, the low abundance of its α elements and neutron-capture elements, along with the high abundance of its iron-peak elements, provides a unique constraint on possible progenitors. We note that a high [Zn/Fe] could be realized by depletion of Fe onto dust grains, as observed for interstellar matter as well as damped Lyman α systems. However, no evidence of such chemical fractionation is seen in the abundance ratio of carbon, which has a lower condensation temperature than Zn, for BS 16920–017. Measurement of S, which has a similar condensation temperature to Zn, would be useful for further confirmation of this point.

The enhancement of iron-peak elements in EMP stars could be explained by hypernovae models, as argued by several recent studies. However, among the iron-peak elements, Mn and Ni, as well as Zn, show particularly large excesses. According to the models of hypernova nucleosynthesis (e.g., Umeda & Nomoto 2002), Zn and Co are enhanced, while no excess is expected for Mn (and Cr). Moreover, it is still unclear if such a very high [Zn/Fe]($\sim +1$) can be explained even by hypernovae models (Tominaga et al. 2007), although N. Tominaga (private communication) suggests

that a high Zn abundance ratio ([Zn/Fe]$\sim$ +0.8) might be realized with a consistent abundance pattern of other elements of BS 16920–017 by a very energetic and bright explosion.

The overall abundance pattern of BS 16920–017 is similar to the few halo stars with exceptionally low abundances of α elements. Ivans et al. (2003) investigated the detailed chemical abundances of three stars having [α/Fe] < 0 at [Fe/H]~ -2. Interestingly, two of them (G 4–36 and CS 22966–043) have significantly high Zn abundance ratios ([Zn/Fe] $\sim +1$; see Figure 2), while the other star (BD +80°245) possesses an under-abundance of Zn ([Zn/Fe] $= -0.4$). Such differences of the abundance ratios between these stars makes it difficult to simply attribute the low abundances of their α elements to large contributions from Type Ia supernovae. The abundance patterns of BS 16920–017 and the two Zn-enhanced objects studied by Ivans et al. (2003) are, at least qualitatively, very similar – significant under-abundances of elements with $Z \leq 20$, large enhancements (with respect to Fe) of Mn and Ni as well as Zn, and deficiencies of heavy neutron-capture elements are among the common features. An important difference of BS 16920–017 from the two objects in Ivans et al. (2003) is its low metallicity ([Fe/H]$= -3.2$). While contributions of at least several supernovae are expected before the formation of metal-poor stars with [Fe/H]$\gtrsim -2$, as is the case for G 4–36 and CS 22966–043, yields from a single supernova are expected to be dominant in the chemical compositions of such EMP stars in the so-called supernova-induced, low-mass star formation scenario (Audouse & Silk 1995; Shigeyama & Tsujimoto 1998). The peculiar abundance of BS 16920–017, including the large Zn excess, would also be explained by a single supernova event.

Under-abundances of α elements are also found in red giants of dwarf spheroidal galaxies, in particular in the metallicity range [Fe/H] > -2. At lower metallicity, the majority of dwarf galaxy stars seem to have over-abundances of their α elements (e.g., Cohen & Huang 2010; Frebel et al. 2010; Norris et al. 2010). However, the Sextans dwarf galaxy, at least, includes EMP stars with abundances of the α elements as low as the solar ratio (Aoki et al. 2009). The [Zn/Fe] ratio in dwarf galaxy stars is, however, not enhanced, or possibly deficient, compared to that of the field halo stars (e.g. Cohen & Huang 2010). This suggests that BS 16920–017 (and probably the Zn-enhanced stars in Ivans et al. (2003)) had quite different origins from those of the currently surviving dwarf spheroidal galaxies, even though both show similarly low abundances of their α elements. We note that Frebel et al. (2010) found a Zn-enhanced EMP star in the UMa II dwarf galaxy. This star (UMa II-S1 : [Fe/H]$= -3.1$) exhibits the highest value of [Zn/Fe] (+0.85), after BS 16920–017, in the abundance studies of EMP stars. However, according to the authors of that paper, the Zn lines of this object are somewhat distorted and the abundance could be overestimated. Hence, this object is excluded in the above comparisons between dwarf spheroidal stars and BS 16920–017.

BS 16920–017 exhibits a high Zn abundance, but shows low abundances of neutron-capture elements. We could not find extreme enhancement of other elements (e.g., [Cu/Fe] $< +0.3$, [Eu/Fe] < 0). Because no neutron-capture element other than Sr and Ba is detected in BS 16920–017, we cannot estimate the relative contributions of r- and s-processes to the neutron-capture elements of this object. The high [Sr/Ba] ratio (+1.3) possibly indicates a contribution of the so-called "weak r-process" (Pfeiffer et al. 2001; Truran et al. 2002; Wanajo & Ishimaru 2006) or the "Light

Element Primary Process" (LEPP: Travaglio et al. 2004; Montes et al. 2007), which has been introduced to explain the high [Sr/Ba] ratios found in some EMP stars (e.g., McWilliam et al. 1995; Burris et al. 2000). Such processes producing large enhancements of light neutron-capture elements (Sr - Zr) do not, however, make an excess of Zn. Indeed, very or extremely metal-poor stars with large enhancements of light neutron-capture elements studied thus far (HD 122563 and HD 88609; Honda et al. 2006, 2007) do not show any excess of Zn. We note that the recent study of Allen & Porto de Mello (2010) suggests that a non-negligible fraction of the synthesis of Zn is due to the weak s-process, based on observations of Ba stars in the metallicity range $-0.7 <$ [Fe/H] $< +0.12$. Yong et al. (2008) found differences in the Zn and Cu abundances in the mildly metal-poor ([Fe/H] $\simeq -1.2$) globular clusters M 4 and M 5, in the sense that the abundances of Zn and Cu in M 4 are enhanced in comparison with those of M 5. Since an excess of s-process-elements in M 4 is also shown by Yong et al. (2008), this process may have influenced the synthesis of Zn. However, the s-process is not expected to contribute significantly to such EMP stars as BS 16920–017 (Kobayashi et al. 2006).

In this study, we determined the behavior of Zn in EMP stars, including the Zn-enhanced star BS 16920–017. The abundance pattern of BS 16920–017 is different from the typical halo EMP stars: it possesses excesses of iron-peak elements, in particular Mn and Ni as well as Zn, with respect to its α elements and neutron-capture elements. This peculiar abundance pattern might be produced by the so-called hypernovae, which are thought to produce large amounts of Zn. Existence of such Zn-enhanced stars suggests that the Zn abundance can be a useful indicator in future "chemical tagging" to distinguish the origins of halo stars based on wide-field spectroscopic surveys.

We would like to thank Dr. N. Tominaga for useful discussions. We also thank an anonymous referee for many helpful comments. S.H., W.A., and M.T.-H are supported by a Grant-in-Aid for Science Research from MEXT (21740148) and from JSPS (18104003 and 22540255). T.C.B. acknowledges partial funding of this work from grants PHY 02-16783 and PHY 08-22648: Physics Frontiers Center/Joint Institute for Nuclear Astrophysics (JINA), awarded by the U.S. National Science Foundation.

REFERENCES

Allen, D. M. & Porto de Mello, G. F. 2010, A&A 525, 63

Allende Prieto, C., Rebolo, R., Garcia Lopez, R. J., Serra-Ricart, M., Beers, T. C., Rossi, S., Bonifacio, P., & Molaro, P. 2000, AJ, 120, 1516

Alonso, A., Arribas, S., & Martinez-Roger, C. 1996, A&AS, 313, 873

Aoki, W., Arimoto, N., Sadakane, K., Tolstoy, E., Battaglia, G., Jablonka, P., Shetrone, M.,

Letarte, B., Irwin, M., Hill, V., Francois, P., Venn, K., Primas, F., Helmi, A., Kaufer, A., Tafelmeyer, M., Szeifert, T., Babusiaux, C. 2009, A&A, 502, 569

Aoki, W., Honda, S., Beers, T. C., Kajino, T., Ando, H., Norris, J. E., Ryan, S. G., Izumiura, H., Sadakane, K., & Takada-Hidai, M. 2005, ApJ, 632, 611 (Paper III)

Aoki, W., Honda, S., Beers, T. C., Takada-Hidai, M., Iwamoto, N., Tominaga, N., Umeda, H., Nomoto, K., Norris, J. E., & Ryan, S. G. 2007, ApJ, 660, 747 (Paper IV)

Asplund, M., Grevesse, N., Sauval, A. J., & Scott P. 2009, ARA&A, 47, 481

Baraffe, I., El Eid, M. F.& Prantzos, N. 1993, A&A, 258, 357

Beers, T. C., & Christlieb, N. 2005, ARAA, 43, 531

Biemont, E., & Godefroid, M. 1980, A&A, 84, 361

Bonifacio, P., et al. 2009, A&A, 501,519

Burris, D. L., Pilachowski, C. A., Armandroff, T. E., Sneden, C., Cowan, J. J., & Roe, H. 2000, ApJ, 544, 302

Cayrel, R., Depagne, E., Spite, M., Hill, V., Spite, F., Francois, P., Beers, T., Primas, F., Andersen, J., Barbuy, B., Bonifacio, P., Molaro, P., & Nordström, B. 2004, A&A, 416, 1117

Cohen, J. G., et al. 2004, ApJ, 612, 1107

Cohen, J. G., & Huang, W. 2010, ApJ, 719, 931

Fröhlich, C., Martínez-Pinedo, G., Liebendörfer, M., Thielemann, F.-K., Bravo, E., Hix, W. R., Langanke, K., & Zinner, N. T. 2006, Phys. Rev. Lett., 96, 142502

François, P., et al. 2007, A&A, 476, 935

Frebel, A., Simon, J. D., Geha, M., & Willman, B. 2010, ApJ, 708, 560

Heger, A., & Woosley, S. E. 2002, ApJ, 567, 532

Heger, A., & Woosley, S. E. 2010, ApJ, 724, 341

Honda, S., et al. 2004a, ApJS, 152, 113 (Paper I)

Honda, S., et al. 2004b, ApJ, 607, 474 (Paper II)

Honda, S., Aoki, W., Ishimaru, Y., Wanajo, S., & Ryan, S. G. 2006, ApJ, 643, 1180

Honda, S., Aoki, W., Ishimaru, Y., & Wanajo, S. 2007, ApJ, 666, 1189

Ivans, I. I., Sneden, C., James, C. R., Preston, G. W., Fulbright, J. P., Höflich, P. A., Carney, B. W., & Wheeler, J. C. 2003, ApJ, 592, 906

Izutani, N., & Umeda, H. 2010, ApJL, 720, 1

Johnson, J. A. 2002, ApJS, 139, 219

Kobayashi, C., Umeda, H., Nomoto, K., Tominaga, N., & Ohkubo, T. 2006, ApJ, 653, 1145

Kurucz, R. L. 1993, CD-ROM 13, ATLAS9 Stellar Atmospheres Programs and 2 km/s Grid (Cambridge: Smithsonian Astrophys. Obs.)

Lai, D. K., Bolte, M., Johnson, J. A., Lucatello, S., Heger, A., & Woosley, S. E. 2008, ApJ, 681, 1524

Matteucci, F., Raiteri, C. M., Busson, M., Gallino, R.& Gratton, R. 1993, A&A, 272, 421

McWilliam, A. 1998, AJ, 115, 1640

McWilliam, A., Preston, G., Sneden, C., & Searle, L. 1995, AJ, 109, 2757

Mishenina, T. V., Kovtyukh, V. V., Soubiran, C., Travaglio, C., & Busso, M. 2002, A&A, 396, 189

Montes, F., Beers, T. C., Cowan, J., Elliot, T., Farouqi, K., Gallino, R., Heil, M., Kratz, K.-L., Pfeiffer, B., Pignatari, M., & Schatz, H. 2007, ApJ, 671, 1685

Nissen, P. E., Akerman, C., Asplund, M., Fabbian, D., Kerber, F., Kaufl, H. U., & Pettini, M. 2007, A&A, 469, 319

Noguchi, K. et al. 2002, PASJ, 54, 855

Norris, J. E., Yong, D., Gilmore, G., & Wyse, R. F. G. 2010, ApJ, 711, 350

Pfeiffer, B., Kratz, K.-L., Thielemann, F.-K.,& Walters, W. B. 2001, Nucl. Phys. A, 693, 282

Pruet, J., Woosley, S. E., Buras, R., Janka, H.-T., & Hoffman, R. D. 2005, ApJ, 623, 325

Primas, F., Brugamyer, E., Sneden, C., King, J.R., Beers, T. C., Boesgaard, A.M., & Deliyannis, C.P. 2000, in The First Stars, ed. AA. Weiss, T. Abel, & V. Hill (Berlin: Springer), 51

Raiteri, C. M., Gallino, R., Busso, M., Neuberger, D.& Käppeler, F. 1993, ApJ, 419, 207

Saito Y.-J., Takada-Hidai M., Honda S., Takeda Y., 2009, PASJ, 61, 549

Sneden, C., et al. 2003, ApJ, 591, 936

Sneden, C., Gratton, R. G., & Crocker, D. A. 1991, A&A, 246, 354

Takeda, Y., Hashimoto, O., Taguchi, H., Yoshioka, K., Takada-Hidai, M., Saito, Y., & Honda, S. 2005, PASJ, 57, 751

Tominaga, N., Umeda, H., & Nomoto, K. 2007, ApJ, 660, 516

Travaglio, C., Gallino, R., Arnone, E., Cowan, J., Jordan, F., & Sneden, C. 2004, ApJ, 601, 864

Truran, J. W., Cowan, J. J., Pilachowski, C. A., & Sneden, C. 2002, PASP, 114, 1293

Umeda, H., & Nomoto, K. 2002, ApJ, 565, 385

Wanajo, S., & Ishimaru, Y. 2006, Nucl. Phys. A, 777, 676

This preprint was prepared with the AAS LaTeX macros v5.2.

Table 1. PROGRAM STARS AND OBSERVATIONS

Star	Wavelength (Å)	Exp.[a] (minutes)	S/N[b] (4000 Å)	(5000 Å)	Obs. date (JD)	Radial velocity (km s^{-1})
BS 16920–017	3500–5100	90 (3)	41/1	59/1	27 Jan.2001 (2451937)	-206.5 ± 0.8
BS 16920–017	4030–6800	30 (1)	40/1[c]	62/1[c]	31 May 2004 (2453156)	-206.2 ± 0.4
HD 4306	3500–5100	30 (2)	272/1	340/1	19 Aug.2000 (2451776)	-69.7 ± 0.3

[a]Total exposure time (number of exposures).

[b]S/N ratio per pixel estimated from the photon counts at around 4000 and 5000 Å.

[c]2×2 binning mode was used.

Table 2. EQUIVALENT WIDTHS OF ZN LINES AND DERIVED ABUNDANCES

	Zn I λ4722	$\log\epsilon$	Zn I λ4810	$\log\epsilon$	$\log\epsilon$(avg.)	[Zn/Fe]	σ
wavelength(Å)	4722.16		4810.54				
$\log gf$	–0.390		–0.170				
L.E.P.(eV)	4.030		4.080				
HD 4306	7.8	2.00	11.6	2.02	2.01	+0.30	0.09
HD 6268	21.3	2.29	23.4	2.17	2.23	+0.30	0.11
HD 88609	10.5	1.92	14.2	1.90	1.91	+0.42	0.20
HD 110184	29.8	2.31	35.6	2.27	2.29	+0.25	0.11
HD 115444	8.8	1.97	11.7	1.94	1.96	+0.25	0.15
HD 122563	15.1	2.11	20.5	2.10	2.11	+0.32	0.19
HD 126587	7.3	2.07	11.0	2.10	2.09	+0.31	0.12
HD 140283	3.1	2.30	5.0	2.34	2.32	+0.29	0.08
HD 186478	20.6	2.41	25.6	2.36	2.39	+0.33	0.12
BS 16082–129	11.6*	2.23*	8.9	1.93	1.93	+0.23	0.15
BS 16085–050	7.6	2.04	8.0	1.89	1.97	+0.32	0.10
BS 16469–075	7.3	2.03	11.9	2.10	2.07	+0.54	0.14
BS 16920–017	20.5	2.41	27.5	2.43	2.42	+1.04	0.23
BS 16928–053	10.1	1.90	14.5	1.92	1.91	+0.26	0.14
CS 22892–052	14.1*	2.25*	9.2	1.87	1.87	+0.23	0.14
CS 22952–015	11.2*	2.16*	8.5	1.84	1.84	+0.22	0.26
CS 30306–132	13.6	2.08	–	–	2.08	–0.06	0.13
CS 31082–001	8.3	1.94	12.2	1.97	1.96	+0.21	0.12

*These values are not used to derive the final results.

Table 3. EQUIVALENT WIDTHS

Species	wavelength	$\log gf$	L.E.P.	HD 4306	$\log \epsilon$	BS 16920–017	$\log \epsilon$	Remarks
Na I	5889.95	0.101	0.000	152 [a]	3.94	109.6 [b]	3.27	
Na I	5895.92	-0.197	0.000	138 [a]	4.00	93.6 [b]	3.21	
Mg I	3829.35	-0.210	2.709	157.6	5.28	110.3	4.72	
Mg I	3832.31	0.140	2.712	190.1	5.25	103.6	4.21	
Mg I	3838.29	0.414	2.717	237.7	5.25	137.1	4.65	
Mg I	4571.10	-5.588	0.000	45.5	5.25	17.5	4.64	
Mg I	5172.68	-0.380	2.712	166 [a]	5.00	131.6	4.80	
Mg I	5183.60	-0.160	2.717	189 [a]	4.98	149.7	4.86	
Mg I	5528.41	-0.490	4.346	52 [a]	5.18	28.8 [b]	4.75	
Al I	3961.53	-0.340	0.010	106.9	3.09	85.1	2.66	
Si I	4102.94	-2.910	1.910	63.0	5.08	22.9	4.23	
Ca I	4283.01	-0.220	1.886	63 [a]	4.29	12.8	3.09	
Ca I	4318.65	-0.210	1.899	47.4	3.96	25.2	3.48	
Ca I	4425.44	-0.360	1.879	42.7	3.98	11.2	3.14	
Ca I	4454.78	0.260	1.899	70.3	3.96	30.8	3.13	
Ca I	5588.75	0.358	2.526	31 [a]	3.69	13.2 [b]	3.18	
Ca I	5594.47	0.097	2.523	–	–	10.5 [b]	3.32	
Ca I	5598.49	-0.087	2.521	–	–	7.2 [b]	3.32	
Ca I	6102.72	-0.770	1.879	24 [a]	3.88	11.6 [b]	3.47	
Ca I	6162.17	0.100	1.899	74 [a]	4.01	31.1 [b]	3.19	
Ca I	6439.08	0.390	2.526	40 [a]	3.79	17.1 [b]	3.25	
Sc II	4400.40	-0.540	0.600	56.2	0.44	27.5 [b]	-0.34	
Sc II	4415.56	-0.670	0.595	48.9	0.42	29.2	-0.18	
Sc II	5031.02	-0.400	1.357	20.3	0.39	8.4	-0.27	
Ti I	3998.64	0.000	0.048	54.8	2.36	–	–	
Ti I	4533.24	0.532	0.848	38.6	2.35	30.0	2.16	
Ti I	4534.78	0.336	0.836	26 [a]	2.26	19.3	2.06	
Ti I	4535.57	0.120	0.826	17 [a]	2.22	14.7	2.12	
Ti I	4981.73	0.560	0.848	44.5	2.39	39.2	2.29	
Ti I	4991.07	0.436	0.836	40.7	2.43	17.8	1.88	
Ti I	4999.50	0.306	0.826	35.8	2.45	25.3	2.20	
Ti I	5039.96	-1.130	0.020	17.3	2.48	12.8	2.30	
Ti I	5064.65	-0.935	0.048	20.5	2.41	18.9 [b]	2.34	

Table 3—Continued

Species	wavelength	log gf	L.E.P.	HD 4306	log ϵ	BS 16920–017	log ϵ	Remarks
Ti I	5173.74	-1.062	0.000	–	–	14.8	2.27	
Ti I	5192.97	-0.948	0.021	17 [a]	2.28	15.5	2.20	
Ti I	5210.38	-0.828	0.048	–	–	17.8 [b]	2.19	
Ti II	4028.36	-1.000	1.892	38.4	2.52	26.8	2.07	
Ti II	4337.88	-1.130	1.080	84.5	2.71	70.2	2.26	
Ti II	4394.07	-1.590	1.220	42.3	2.35	28.6 [b]	1.87	
Ti II	4395.85	-1.970	1.243	30.6	2.52	25.1 [b]	2.19	
Ti II	4399.79	-1.270	1.237	74.5	2.75	57.3 [b]	2.22	
Ti II	4417.72	-1.430	1.165	73.9	2.81	63.4	2.44	
Ti II	4443.78	-0.700	1.080	96.8	2.58	87.7	2.31	
Ti II	4450.50	-1.510	1.084	64.7	2.56	58.1	2.28	
Ti II	4464.46	-2.080	1.161	44.8	2.81	38.5	2.50	
Ti II	4468.52	-0.600	1.131	98.4	2.57	89.3	2.31	
Ti II	4470.84	-2.280	1.165	28.1	2.67	24.5	2.38	
Ti II	4501.27	-0.760	1.116	93.9	2.58	83.0	2.26	
Ti II	4571.96	-0.530	1.572	85.8	2.66	76.8	2.37	
Ti II	4589.92	-1.790	1.237	48.4	2.66	41.6	2.35	
Ti II	4865.61	-2.810	1.116	11.3	2.61	10.3 [b]	2.35	
Ti II	5129.16	-1.390	1.892	31 [a]	2.64	20.6	2.19	
Ti II	5185.90	-1.350	1.893	22 [a]	2.39	17.9	2.07	
Ti II	5188.69	-1.210	1.582	54 [a]	2.53	49.0	2.27	
Ti II	5226.54	-1.300	1.566	44 [a]	2.41	45.9 [b]	2.27	
Ti II	5336.78	-1.630	1.582	30 [a]	2.47	27.3 [b]	2.21	
V I	4379.23	0.550	0.301	14.2	1.08	5.6 [b]	0.59	
V II	3951.96	-0.784	1.476	17.7	1.22	–	–	
V II	4005.71	-0.522	1.820	18.1	1.37	17.6	1.15	
Cr I	4254.33	-0.114	0.000	82 [a]	2.28	82.9	2.50	
Cr I	4274.81	-0.321	0.000	103 [a]	3.08	79.6	2.59	
Cr I	4289.72	-0.360	0.000	85.9	2.63	72.9	2.41	
Cr I	5204.51	-0.208	0.941	–	–	67.0 [b]	3.00	
Cr I	5206.04	0.019	0.941	63 [a]	2.60	58.9 [b]	2.56	
Cr I	5208.44	0.160	0.940	76 [a]	2.75	68.8 [b]	2.68	
Cr II	4558.65	-0.660	4.070	10.2	3.00	8.9	2.72	

Table 3—Continued

Species	wavelength	log gf	L.E.P.	HD 4306	log ϵ	BS 16920–017	log ϵ	Remarks
Cr II	4588.20	-0.630	4.070	8.4	2.87	4.1	2.32	
Mn I	4030.75	-0.470	0.000	91.0	1.50	98.7	1.69	
Mn I	4033.06	-0.618	0.000	77.4	1.51	86.7	1.73	
Mn I	4034.48	-0.811	0.000	79.1	1.83	80.8	1.92	
Mn I	4041.36	0.285	2.114	16.6	2.05	31.8	2.45	no HF
Mn I	4754.05	-0.086	2.282	6.3	2.07	13.5	2.39	
Mn I	4823.53	0.144	2.319	8.8	2.04	13.3	2.21	
Fe I	3763.80	-0.240	0.990	139.0	4.59	98.0	4.03	
Fe I	3767.19	-0.390	1.010	125.9	4.58	90.8	3.99	
Fe I	3787.88	-0.859	1.011	112.0	4.76	85.3	4.25	
Fe I	3805.34	0.310	3.301	46.8	4.41	–	–	
Fe I	3815.84	0.226	1.485	137.2	4.62	96.9	4.06	
Fe I	3820.43	0.120	0.860	188.2	4.46	149.9	4.30	
Fe I	3825.88	-0.024	0.920	165.1	4.51	131.0	4.28	
Fe I	3827.82	0.062	1.557	124.3	4.68	107.9	4.58	
Fe I	3840.44	-0.506	0.990	123.9	4.56	92.1	4.04	
Fe I	3849.98	-0.863	1.010	110.6	4.67	99.5	4.62	
Fe I	3856.37	-1.280	0.052	137.6	4.67	123.1	4.71	
Fe I	3859.91	-0.710	0.000	184.0	4.53	142.5	4.40	
Fe I	3865.52	-0.982	1.011	111.2	4.79	90.4	4.47	
Fe I	3886.28	-1.080	0.050	115.4	4.00	125.8	4.56	
Fe I	3899.71	-1.531	0.087	127.7	4.75	118.0	4.88	
Fe I	3902.95	-0.466	1.557	103.8	4.73	92.4	4.66	
Fe I	3920.26	-1.746	0.121	121.8	4.87	114.1	5.02	
Fe I	3922.91	-1.651	0.052	128.9	4.84	114.2	4.85	
Fe I	3949.95	-1.250	2.176	45.5	4.61	26.8	4.18	
Fe I	4005.24	-0.610	1.557	101.5	4.79	85.0	4.54	
Fe I	4063.59	0.060	1.557	128.4	4.68	110.3	4.57	
Fe I	4071.74	-0.022	1.608	120.6	4.67	98.0 [b]	4.38	
Fe I	4076.63	-0.530	3.210	26.7	4.64	12.4 [b]	4.18	
Fe I	4114.45	-1.300	2.832	12.8	4.55	–	–	
Fe I	4132.90	-1.010	2.845	23.1	4.61	12.4 [b]	4.24	
Fe I	4143.87	-0.510	1.557	104.0	4.69	102.3	4.91	

Table 3—Continued

Species	wavelength	$\log gf$	L.E.P.	HD 4306	$\log \epsilon$	BS 16920–017	$\log \epsilon$	Remarks
Fe I	4147.67	-2.104	1.485	47.5	4.66	30.9	4.49	
Fe I	4154.50	-0.690	2.832	38.1	4.62	15.7 [b]	4.02	
Fe I	4156.81	-0.810	2.832	39.6	4.77	17.5 [b]	4.20	
Fe I	4157.78	-0.400	3.417	27.8	4.77	–	–	
Fe I	4174.91	-2.970	0.920	41.9	4.73	30.9	4.49	
Fe I	4175.64	-0.830	2.845	30.1	4.60	–	–	
Fe I	4181.76	-0.370	2.832	53.2	4.63	38.7 [b]	4.32	
Fe I	4182.38	-1.180	3.017	8.6	4.44	–	–	
Fe I	4187.04	-0.548	2.450	64.7	4.64	44.4	4.20	
Fe I	4187.79	-0.550	2.420	66.5	4.66	54.6	4.43	
Fe I	4191.43	-0.670	2.469	54.7	4.54	41.8	4.28	
Fe I	4195.33	-0.490	3.332	30.5	4.82	7.8 [b]	4.04	
Fe I	4199.10	0.160	3.047	61.0	4.54	38.0	4.03	
Fe I	4202.03	-0.689	1.490	102.3	4.74	94.2	4.76	
Fe I	4222.21	-0.967	2.450	45.6	4.60	29.9	4.26	
Fe I	4227.43	0.270	3.332	–	–	40.2	4.30	
Fe I	4233.60	-0.604	2.482	–	–	58.9	4.67	
Fe I	4250.12	-0.405	2.469	–	–	46.7	4.12	
Fe I	4250.79	-0.710	1.557	–	–	87.6	4.63	
Fe I	4260.47	0.080	2.399	–	–	79.9	4.55	
Fe I	4271.15	-0.349	2.450	–	–	52.3 [b]	4.17	
Fe I	4325.76	0.010	1.608	125.6	4.67	123.8	4.89	
Fe I	4337.05	-1.695	1.557	62.1	4.64	40.4 [b]	4.16	
Fe I	4383.56	0.208	1.490	143.6	4.58	127.8 [b]	4.58	
Fe I	4404.76	-0.147	1.560	123.3	4.68	101.5 [b]	4.41	
Fe I	4415.14	-0.621	1.610	104.0	4.77	100.3	4.90	
Fe I	4430.61	-1.659	2.223	26.7	4.60	–	–	
Fe I	4442.34	-1.255	2.198	49.3	4.64	32.8	4.29	
Fe I	4443.19	-1.040	2.858	18.9	4.51	16.5 [b]	4.41	
Fe I	4447.72	-1.342	2.223	44.7	4.66	23.0	4.16	
Fe I	4466.55	-0.600	2.832	49.3	4.74	28.6	4.28	
Fe I	4489.74	-3.966	0.121	40.3	4.70	28.0 [b]	4.41	
Fe I	4494.56	-1.136	2.198	54.9	4.64	41.6	4.37	

Table 3—Continued

Species	wavelength	log gf	L.E.P.	HD 4306	log ϵ	BS 16920–017	log ϵ	Remarks
Fe I	4528.61	-0.822	2.176	71.0	4.66	57.2	4.40	
Fe I	4531.15	-2.155	1.485	48.9	4.69	31.7	4.32	
Fe I	4602.94	-2.210	1.485	46.3	4.68	30.8	4.34	
Fe I	4736.77	-0.750	3.210	23.1	4.72	12.2	4.35	
Fe I	4871.32	-0.362	2.870	51.2	4.53	37.6	4.26	
Fe I	4872.14	-0.570	2.882	41.5	4.56	29.7	4.30	
Fe I	4890.76	-0.390	2.876	51.0	4.56	32.3	4.17	
Fe I	4891.49	-0.110	2.851	64.5	4.55	48.8	4.24	
Fe I	4903.31	-0.930	2.882	25.6	4.57	15.3	4.26	
Fe I	4918.99	-0.340	2.865	52.7	4.53	37.1	4.22	
Fe I	4924.77	-2.256	2.279	10.1	4.69	6.8 [b]	4.46	
Fe I	4938.81	-1.080	2.876	18.5	4.52	12.3	4.28	
Fe I	4939.69	-3.340	0.859	30.0	4.69	20.8	4.44	
Fe I	4946.39	-1.170	3.368	7.2	4.70	–	–	
Fe I	4966.09	-0.870	3.332	13.9	4.68	8.7	4.42	
Fe I	4973.10	-0.950	3.960	3.8	4.86	–	–	
Fe I	4994.13	-2.956	0.915	39.8	4.57	31.0	4.37	
Fe I	5001.87	0.050	3.880	16.6	4.49	10.6	4.23	
Fe I	5006.12	-0.610	2.833	42.5	4.54	28.4	4.24	
Fe I	5014.94	-0.300	3.943	10.2	4.65	–	–	
Fe I	5022.24	-0.530	3.984	6.4	4.71	–	–	
Fe I	5041.76	-2.200	1.485	52.1	4.73	33.2	4.34	
Fe I	5044.21	-2.040	2.850	3.8	4.66	–	–	
Fe I	5049.82	-1.344	2.279	39.5	4.56	27.0	4.28	
Fe I	5051.64	-2.795	0.915	56.9	4.74	44.0	4.49	
Fe I	5068.77	-1.040	2.940	17.1	4.50	14.2	4.38	
Fe I	5074.75	-0.200	4.220	8.0	4.75	–	–	
Fe I	5083.34	-2.958	0.958	44.1	4.70	31.3	4.42	
Fe I	5090.77	-0.360	4.256	4.5	4.67	–	–	
Fe I	5123.73	-3.068	1.011	–	–	26.6	4.48	
Fe I	5127.37	-3.307	0.915	–	–	17.6	4.36	
Fe I	5150.84	-3.003	0.990	–	–	20.2	4.22	
Fe I	5151.91	-3.322	1.011	–	–	16.8	4.47	

Table 3—Continued

Species	wavelength	$\log gf$	L.E.P.	HD 4306	$\log \epsilon$	BS 16920–017	$\log \epsilon$	Remarks
Fe I	5162.27	0.020	4.178	–	–	10.1	4.57	
Fe I	5171.60	-1.793	1.485	–	–	58.3	4.49	
Fe I	5191.46	-0.550	3.038	–	–	19.7	4.18	
Fe I	5192.34	-0.420	2.998	–	–	26.0	4.17	
Fe I	5194.94	-2.090	1.557	–	–	37.8	4.40	
Fe II	4178.86	-2.480	2.583	41.2	4.77	21.3 [b]	4.11	
Fe II	4233.17	-2.000	2.583	–	–	42.9 [b]	4.15	
Fe II	4416.82	-2.600	2.778	21.2	4.63	10.6 [b]	4.05	
Fe II	4491.40	-2.700	2.856	15.8	4.66	8.6	4.13	
Fe II	4508.28	-2.580	2.856	26.6	4.84	18.4	4.41	
Fe II	4515.34	-2.480	2.844	22.3	4.61	16.0	4.22	
Fe II	4520.22	-2.600	2.810	21.3	4.67	12.3	4.16	
Fe II	4541.52	-3.050	2.856	7.7	4.64	–	–	
Fe II	4555.89	-2.290	2.828	26.7	4.51	–	–	
Fe II	4576.33	-2.940	2.844	9.0	4.59	–	–	
Fe II	4583.83	-2.020	2.807	53.2	4.78	41.9	4.38	
Fe II	4923.93	-1.320	2.891	73.7	4.58	70.0	4.41	
Fe II	4993.35	-3.670	2.810	1.8	4.50	–	–	
Fe II	5018.44	-1.292	2.890	84.4	4.78	77.3	4.55	
Co I	3842.05	-0.770	0.923	32.9	2.24	27.9	2.10	
Co I	3845.47	0.010	0.923	63.3	2.19	48.2	1.84	
Co I	3873.12	-0.660	0.432	96.0	3.33	63.2	2.40	not used
Co I	3881.87	-1.130	0.582	43.2	2.42	38.7	2.32	
Co I	3995.31	-0.220	0.923	59.0	2.26	49.3	2.07	
Co I	4020.90	-2.070	0.432	13.7	2.40	–	–	
Co I	4110.53	-1.080	1.049	12.6	2.09	–	–	
Co I	4121.32	-0.320	0.923	62.9	2.43	54.9	2.30	
Ni I	3807.14	-1.220	0.423	85.3	3.39	83.1	3.56	
Ni I	3858.30	-0.951	0.423	93.0	3.34	89.5	3.48	
Ni I	5476.90	-0.890	1.826	45 [a]	3.32	51.4 [b]	3.46	
Ni I	6643.64	-2.300	1.676	–	–	9.9 [b]	3.52	
Ni I	6767.78	-2.170	1.826	–	–	7.0 [b]	3.40	
Cu I	5105.55	-1.520	1.390	syn	<0.94	syn	<1.31	

Table 3—Continued

Species	wavelength	$\log gf$	L.E.P.	HD 4306	$\log \epsilon$	BS 16920–017	$\log \epsilon$	Remarks
Zn I	4722.15	-0.390	4.030	7.8	2.00	20.5	2.41	
Zn I	4810.53	-0.170	4.078	11.6	2.02	27.5 [b]	2.43	
Sr II	4077.72	0.150	0.000	121.0	-0.09	86.5 [b]	-0.87	
Sr II	4215.54	-0.180	0.000	117 [a]	0.12	86.0	-0.62	
Ba II	4554.04	0.170	0.000	20.2	-1.81	20.2	-2.74	
Ba II	4934.10	-0.150	0.000	46.0	-1.77	13.3	-2.68	
Eu II	3819.67	0.510	0.000	syn	-2.98	–	–	
Eu II	4129.72	0.220	0.000	syn	-2.78	syn	< -2.66	
Eu II	4205.05	0.210	0.000	syn	-3.00	–	–	

[a]Taken from McWilliam et al (1995).

[b]Measured for the spectrum obtained in 2004.

Table 4. ADOPTED ATMOSPHERIC PARAMETERS

Star	$T_{\rm eff}$(K)	$\log g$	[Fe/H]	$v_{\rm micro}$(km s^{-1})
BS 16920–017	4760	1.2	−3.12	1.4
HD 4306	4810	1.8	−2.89	1.6

Table 5. ABUNDANCE RESULTS

Element	Species	Solar Abundance[a]	HD 4306				BS 16920–017			
		$\log \epsilon$	$\log \epsilon$	[X/Fe]	N	σ	$\log \epsilon$	[X/Fe]	N	σ
C	CH [b]	8.43	5.78	+0.20	···	···	5.37	+0.12	···	···
Na	Na I	6.24	3.97	+0.58	2	···	3.24	+0.18	2	···
Mg	Mg I	7.60	5.17	+0.42	7	0.13	4.66	+0.24	7	0.21
Al	Al I	6.45	3.09	−0.51	1	···	2.66	−0.61	1	···
Si	Si I	7.51	5.08	+0.42	1	···	4.23	−0.10	1	···
Ca	Ca I	6.34	3.94	+0.45	8	0.18	3.26	+0.10	10	0.14
Sc	Sc II	3.15	0.42	+0.12	3	0.03	−0.26	−0.23	3	0.08
Ti	Ti I	4.95	2.36	+0.26	10	0.08	2.18	+0.41	11	0.13
Ti	Ti II	4.95	2.59	+0.49	20	0.13	2.26	+0.49	20	0.14
V	V I	3.93	1.08	0.00	1	···	0.59	−0.16	1	···
V	V II	3.93	1.30	+0.22	2	···	1.15	+0.40	1	···
Cr	Cr I	5.64	2.67	−0.12	5	0.29	2.62	+0.16	6	0.20
Cr	Cr II	5.64	2.94	+0.15	2	···	2.52	+0.06	2	···
Mn	Mn I	5.43	1.83	−0.75	6	0.27	2.07	−0.18	6	0.33
Fe	Fe I	7.50	4.64	−2.86 [c]	82	0.12	4.38	−3.12 [c]	84	0.22
Fe	Fe II	7.50	4.66	−2.84 [c]	13	0.11	4.26	−3.24 [c]	10	0.17
Co	Co I	4.99	2.29	+0.15	7	0.13	2.13	+0.32	5	0.20
Ni	Ni I	6.22	3.35	−0.02	3	0.03	3.48	+0.44	5	0.06
Cu	Cu I	4.19	<0.94	< −0.40	1	···	<1.31	<+0.30	1	···
Zn	Zn I	4.56	2.01	+0.30	2	···	2.42	+1.04	2	···
Sr	Sr II	2.87	0.02	0.00	2	···	−0.75	−0.44	2	···
Ba	Ba II	2.18	−1.79	−1.12	2	···	−2.71	−1.71	2	···
Eu	Eu II	0.52	−2.92	−0.59	3	0.12	< −2.66	<+0.00	1	···

[a]Asplund et al. (2009)

[b]Derived from the CH 4320 Å band

[c][Fe/H] values

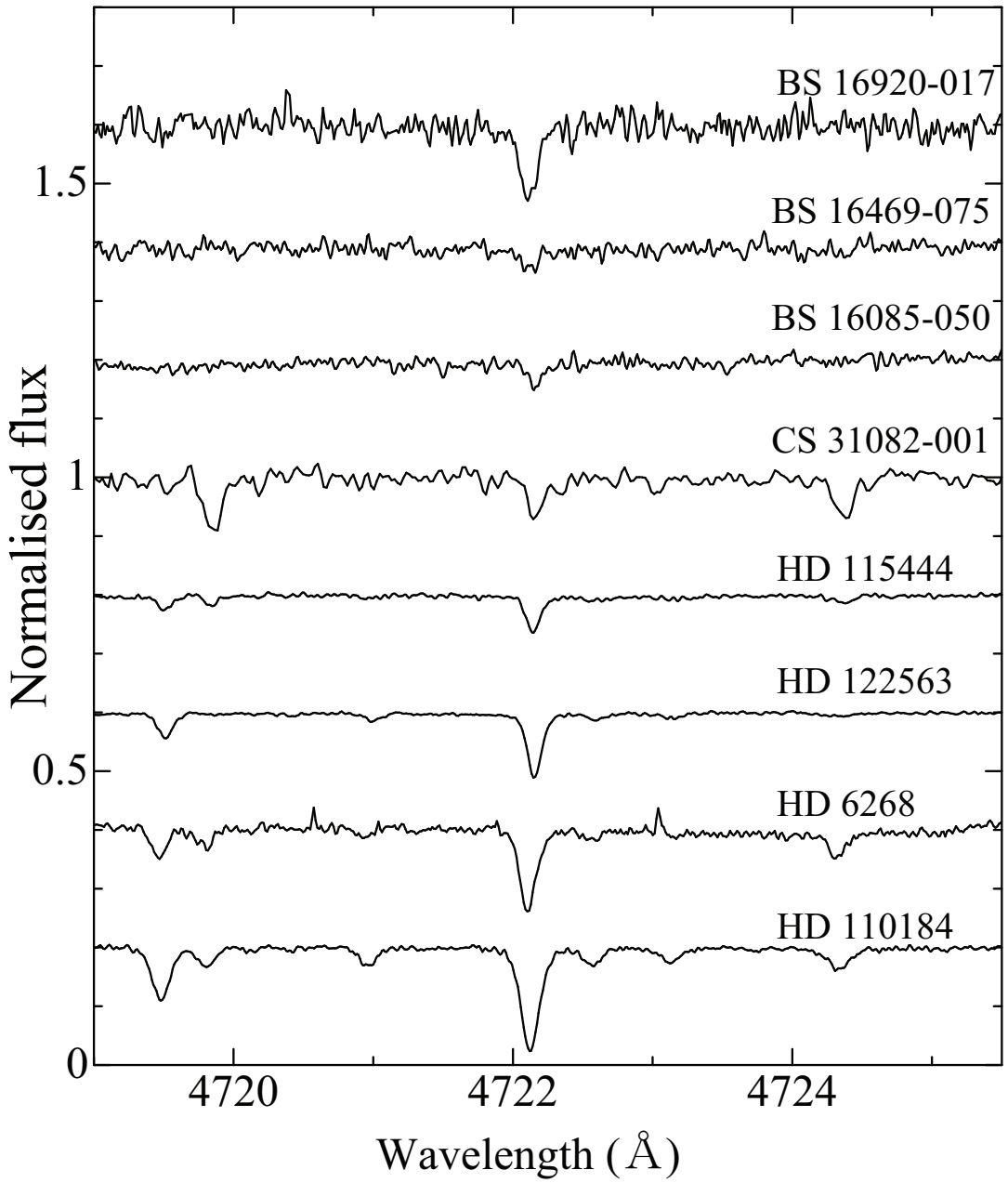

Fig. 1.— Examples of observed spectra in the vicinity of the Zn I 4722 Å line. A vertical offset is applied between the spectra.

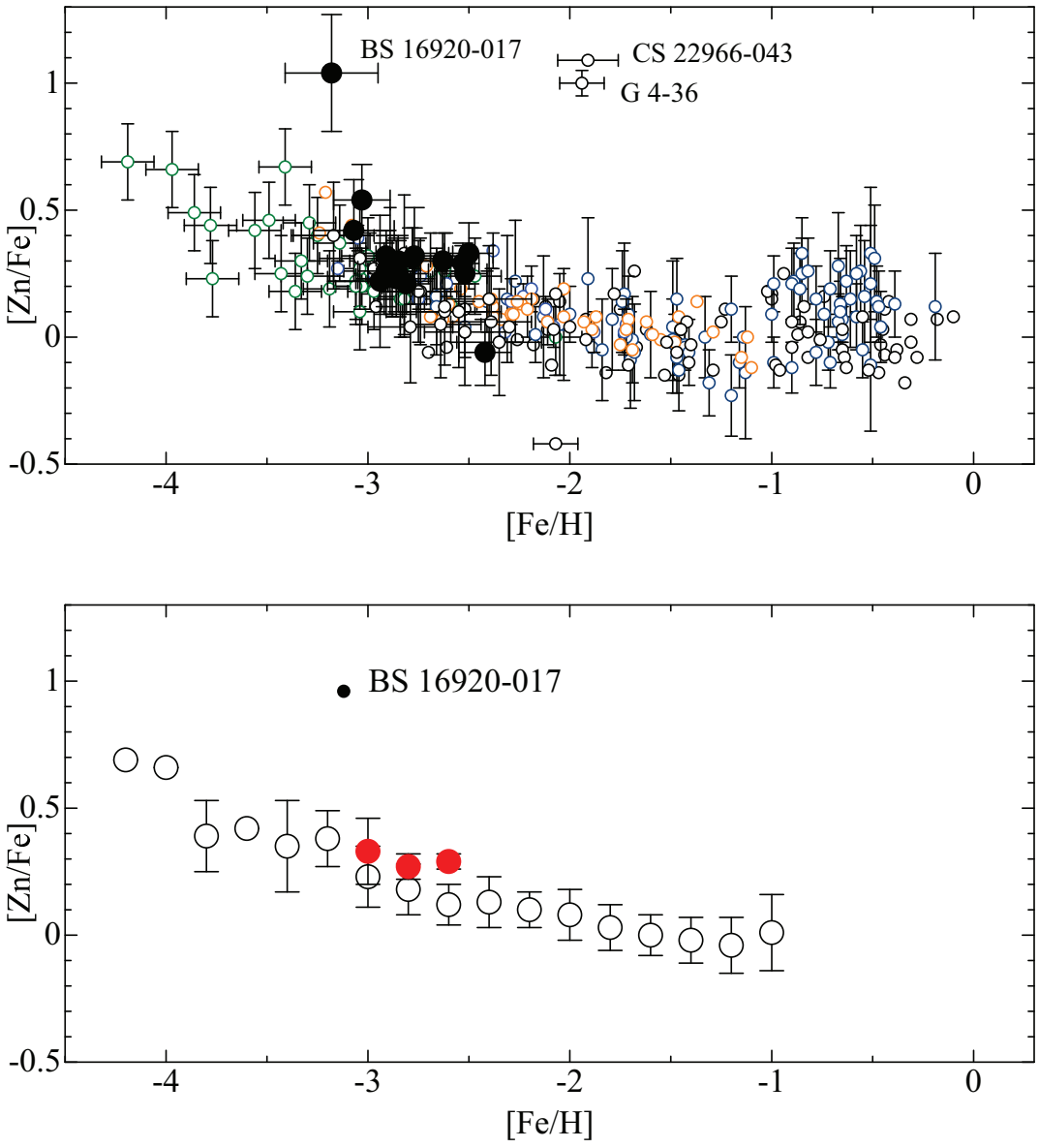

Fig. 2.— *Upper panel*: [Zn/Fe] abundance ratios as a function of [Fe/H] for our sample stars (filled circles). Results of previous studies are shown by open circles (Sneden et al. 1991; Johnson 2002; Mishenina et al. 2002; Ivans et al. 2003; Cayrel et al. 2004; Aoki et al. 2005; Nissen et al. 2007; Saito et al. 2009). *Lower panel*: The average [Zn/Fe] abundance ratios in 0.2 dex bins of [Fe/H] are shown by large filled circles for our sample and by open circles for those of previous studies. The bar indicates the standard deviation of the [Zn/Fe] values of each bin. The data of BS 16920–017 is not included in the statistics.

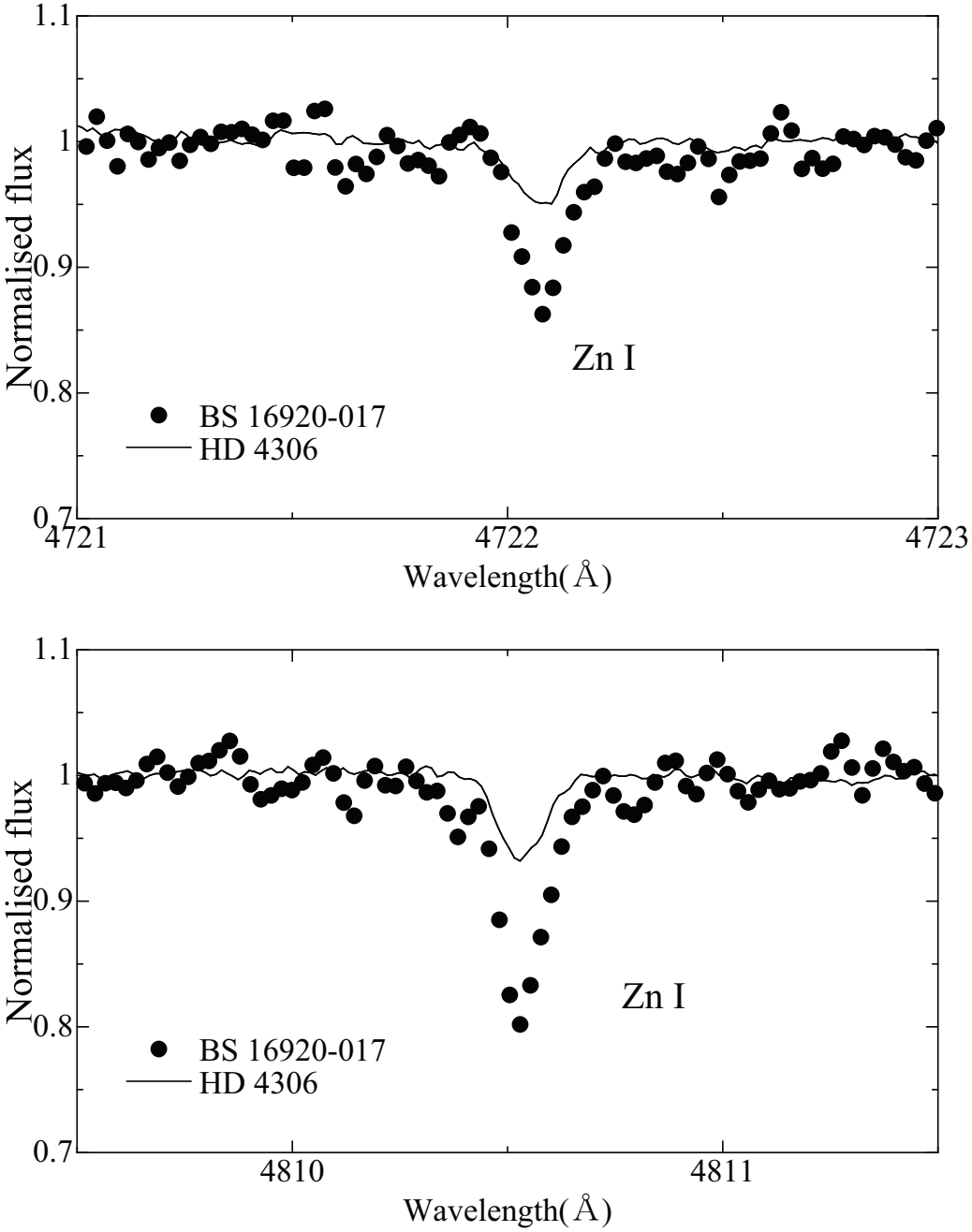

Fig. 3.— Comparison of the spectra of the Zn λ4722 Å line in BS 16920–017 (filled circles) and HD 4306 (solid line). Although the metallicity of HD 4306 is higher than BS 16920–017, the Zn line is clearly stronger in BS 16920–017.

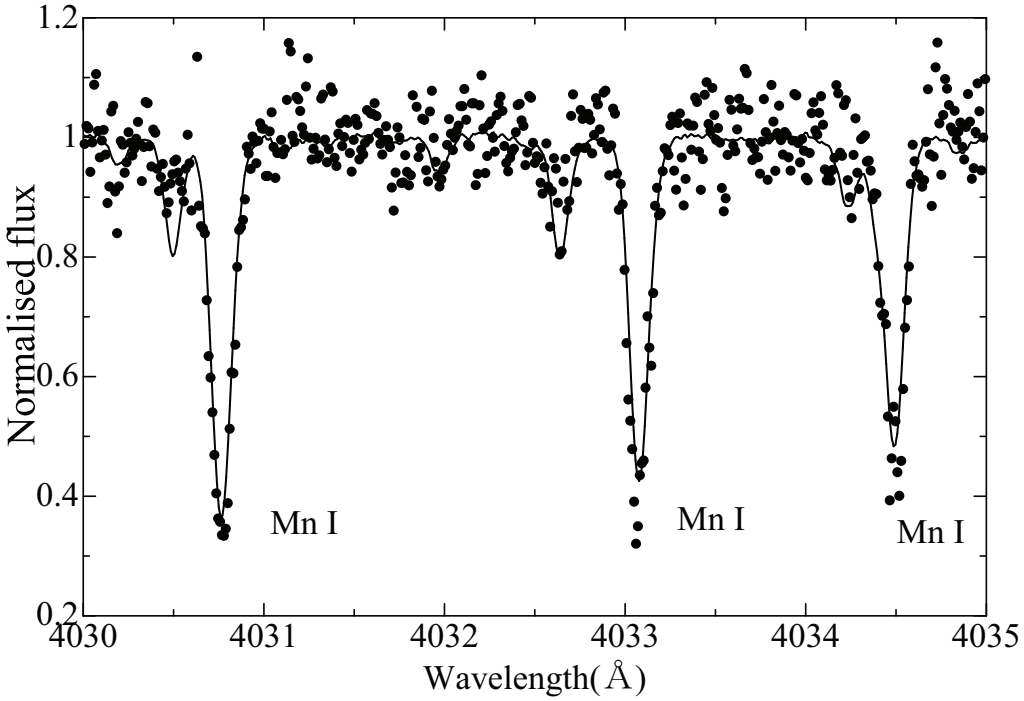

Fig. 4.— Comparison of the spectra of the Mn lines in BS 16920–017 (filled circles) and HD 4306 (solid line). Although the metallicity of HD 4306 is higher than BS 16920–017, two of the three Mn lines are clearly stronger in BS 16920–017.

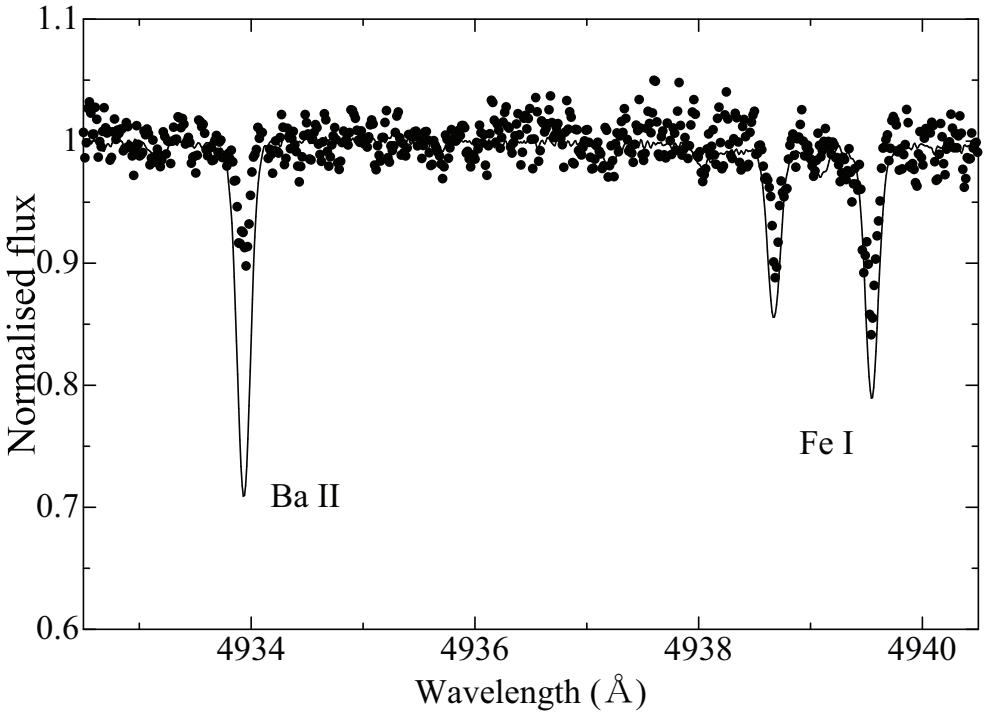

Fig. 5.— Comparison of the spectra of the Ba and Fe lines in BS 16920–017 (filled circles) and HD 4306 (solid line). The Ba line of BS 16920–017 is significantly weaker than that of HD 4306.

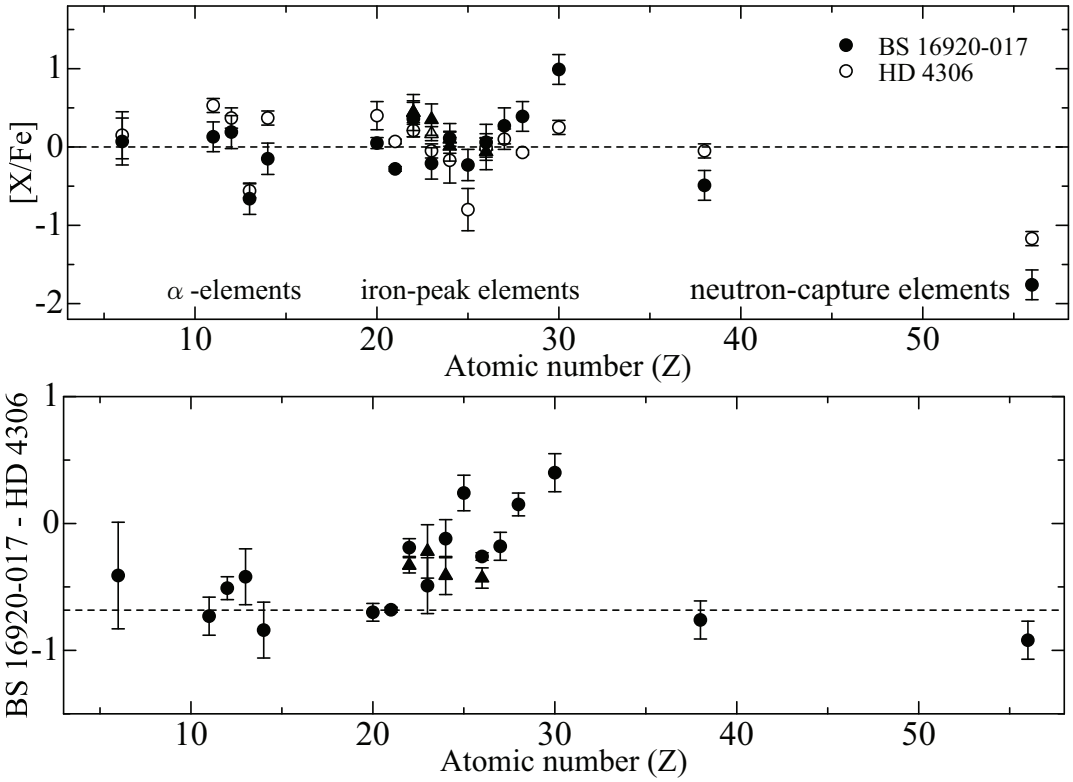

Fig. 6.— *Upper panel*: Comparisons of the abundance ratios, [X/Fe], as a function of the atomic number (Z), for BS 16920–017 (filled circles and triangles) and HD 4306 (open circles and triangles). The circles indicate abundances derived from neutral species and triangles indicate those from ionized species (for Ti, V, Cr, and Fe). The dashed line is a reference at [X/Fe] = 0.0. *Lower panel*: Abundance differences, on the logarithmic scale, between the two stars. The dashed line indicates the average of the values of the α elements (Mg, Si, and Ca).